A COMPARATIVE STUDY OF FUSION-BASED CHANGE DETECTION METHODS FOR MULTI-BAND IMAGES WITH DIFFERENT SPECTRAL AND SPATIAL RESOLUTIONS

Vinicius Ferraris[(1)], *Naoto Yokoya*[(2)], *Nicolas Dobigeon*[(1)] *and Marie Chabert*[(1)]

[(1)] University of Toulouse, IRIT/INP-ENSEEIHT, Toulouse, France
[(2)] Geoinformatics Unit, RIKEN Center for Advanced Intelligence Project, Japan
`firstname.lastname@enseeiht.fr, naoto.yokoya@riken.jp`

ABSTRACT

This paper deals with a fusion-based change detection (CD) framework for multi-band images with different spatial and spectral resolutions. The first step of the considered CD framework consists in fusing the two observed images. The resulting fused image is subsequently spatially or spectrally degraded to produce two pseudo-observed images, with the same resolutions as the two observed images. Finally, CD can be performed through a pixel-wise comparison of the pseudo-observed and observed images since they share the same resolutions. Obviously, fusion is a key step in this framework. Thus, this paper proposes to quantitatively and qualitatively compare state-of-the-art fusion methods, gathered into four main families, namely component substitution, multi-resolution analysis, unmixing and Bayesian, with respect to the performance of the whole CD framework evaluated on simulated and real images.

Index Terms— Change detection, hyperspectral and multispectral imaging, fusion, heterogeneous sensors.

1. INTRODUCTION

Change detection (CD) compares images acquired over the same geographical spot at different times. The objective is to generate a map representing the portions of the scene that have changed between the acquisitions. Most CD methods [1] rely on the practical scenario whereby images to be compared are of the same modalities (optical, radar) and of same spatial and spectral resolutions, e.g., panchromatic (PAN), multispectral (MS) or hyperspectral (HS). Under this scenario, CD is obtained through a pixel-wise comparison of the two images. The operations involved in this comparison depend upon the considered modality. In a nutshell, this comparison is mainly based upon differences (respectively ratios) in the case of optical (respectively SAR) images. Note that the majority of existing CD methods are devoted to this scenario. However, this scenario is not representative of all the situations where CD must be addressed [2]. Natural disasters, punctual missions, defense and security are examples where CD should handle images with different resolutions and possibly of different modalities. Robust and reliable CD methods tailored to these situations are thus needed. Recently, new approaches [2, 3] have been proposed to deal with images of the same modality but with different resolutions. Both approaches consists in fusing the two observed images to produce a fused image of high spatial and

spectral resolution. In [2], two pseudo-observed images, with the same resolutions as the two observed images, are subsequently derived by degrading the fused image. Then, CD can be classically performed through a pixel-wise comparison of the pseudo-observed and observed images sharing the same resolutions. Note that the final change map possesses the same high resolution as the fused image. Consequently, these approaches have a comparative advantage over state-of-the-art techniques, which individually and independently resample the observed images to a common (low) resolution, leading to a change map with low resolution. Moreover, each step of the framework proposed in [2] (fusion, prediction and pixel-wise change detection) can be tailored by the end-user, bringing an additional flexibility to the method. Consequently, this paper exploits this flexibility by experimenting the most powerful state-of-the-art fusion methods in the case of PAN, MS and HS images. Indeed, these image modalities are ubiquitous since, according to the UCS Satellite Database [4], the majority of Earth observation satellites are embedded with (multiband) optical sensors. For that reason, [5] has proposed a deep comparative study on the state-of-the-art MS and HS data fusion methods, gathered into 4 main families, namely component substitution (CS), multi-resolution analysis (MRA), spectral unmixing and Bayesian techniques. This paper proposes to compare the performance of the whole CD framework when the fusion step is conducted by one algorithm chosen in each of these fusion families. Section 2 briefly recalls the CD framework proposed in [2]. Section 3 describes the state-of-the-art fusion methods that will be incorporated into the CD framework. Section 4 analyzes the CD performance obtained through simulated and real images when considering these algorithms as the fusion step. Conclusions are reported in Section 5.

2. CHANGE DETECTION: A FUSION-BASED APPROACH

2.1. Forward model and change hypothesis

Let consider two observed multi-band optical images acquired over the same geographical spot at two different times t_i and t_j. Without loss of generality, assume that the image acquired at time t_i is a high spatial low spectral resolution (HR) image and the one acquired at time t_j is a low spatial high spectral resolution (LR) image denoted respectively by $\mathbf{Y}_{\mathrm{HR}}^{t_i} \in \mathbb{R}^{n_\lambda \times n}$ and $\mathbf{Y}_{\mathrm{LR}}^{t_j} \in \mathbb{R}^{m_\lambda \times m}$ where n_λ (resp., m_λ) and n (resp. m) denote the numbers of bands and pixels of the HR (resp. LR) images with $m_\lambda > n_\lambda$ and $n > m$. These observed images can be seen as the individual results of two degradations of two (unobserved) high spatial and spectral resolution latent images $\mathbf{X}^{t_k} \in \mathbb{R}^{m_\lambda \times n}$ ($k = i, j$) by two operators denoted by $T_{\mathrm{HR}}[\cdot]$ and $T_{\mathrm{LR}}[\cdot]$, respectively. Note that the two unobserved la-

tent images are assumed to share the same spatial and spectral characteristics. When the two observed images have been acquired at the same time, i.e., $t_i = t_j$, no change is expected and the latent images $\mathbf{X}^{t_i}$ and $\mathbf{X}^{t_j}$ should represent exactly the same scene, i.e., $\mathbf{X}^{t_i} = \mathbf{X}^{t_j} \triangleq \mathbf{X}$. Recovering an estimate $\hat{\mathbf{X}}$ of $\mathbf{X}$ from $\mathbf{Y}_{\text{HR}}^{t_i}$ and $\mathbf{Y}_{\text{LR}}^{t_j}$ can be cast as a fusion problem. However, when $t_i \neq t_j$, changes may have occurred meanwhile. Thus, no common latent image $\mathbf{X}$ can be defined since $\mathbf{X}^{t_i} \neq \mathbf{X}^{t_j}$. However, since $\mathbf{X}^{t_i}$ and $\mathbf{X}^{t_j}$ represent the same area of interest, they are expected to keep a certain level of similarity. Therefore, the fusion process does not lead to a common latent image anymore, but to a pseudo-latent image $\hat{\mathbf{X}}$ from the observed image pair $\mathbf{Y}_{\text{HR}}^{t_i}$ and $\mathbf{Y}_{\text{LR}}^{t_j}$. The pseudo-latent image can be interpreted as the best joint approximation of latent images $\mathbf{X}^{t_i}$ and $\mathbf{X}^{t_j}$. The no-change hypothesis $\mathcal{H}_0$ corresponding to the case of a perfect fusion process, and the change hypothesis $\mathcal{H}_1$ can be formulated as, respectively,

$$\mathcal{H}_0 : \left\{ \begin{array}{ccc} \mathbf{Y}_{\text{HR}}^{t_i} & = & \hat{\mathbf{Y}}_{\text{HR}}^{t_i} \\ \mathbf{Y}_{\text{LR}}^{t_j} & = & \hat{\mathbf{Y}}_{\text{LR}}^{t_j} \end{array} \right. \quad \mathcal{H}_1 : \left\{ \begin{array}{ccc} \mathbf{Y}_{\text{HR}}^{t_i} & \neq & \hat{\mathbf{Y}}_{\text{HR}}^{t_i} \\ \mathbf{Y}_{\text{LR}}^{t_j} & \neq & \hat{\mathbf{Y}}_{\text{LR}}^{t_j} \end{array} \right. \quad (1)$$

where

$$\hat{\mathbf{Y}}_{\text{HR}}^{t_i} \triangleq T_{\text{HR}} \left[\hat{\mathbf{X}} \right], \quad \hat{\mathbf{Y}}_{\text{LR}}^{t_j} \triangleq T_{\text{LR}} \left[\hat{\mathbf{X}} \right] \quad (2)$$

are the two predicted HR and LR images from the estimated pseudo-latent image $\hat{\mathbf{X}}$.

Note that the equalities/inequalities in (1) should be considered pixel by pixel, leading to a change/no change decision for each pixel of the HR and LR images. The majority of the fused image pixels correspond to the truly observed scene. The few remaining ones, corresponding to locations impacted by the changes, are expected to suffer from spatial and spectral aberrations due to the inconsistency of the information between the two observed images. Note that the pixel-wise rules to decide between $\mathcal{H}_0$ and $\mathcal{H}_1$ provide two change maps with the same resolution as the HR and LR images.

2.2. 3-Step Framework

Capitalizing on the aforementioned forward model and change hypothesis, the CD framework proposed in [2] mainly consists of the following three steps:

1. *fusion*: estimating $\hat{\mathbf{X}}$ from $\mathbf{Y}_{\text{HR}}^{t_1}$ and $\mathbf{Y}_{\text{LR}}^{t_2}$,

2. *prediction*: reconstructing $\hat{\mathbf{Y}}_{\text{HR}}^{t_1}$ and $\hat{\mathbf{Y}}_{\text{LR}}^{t_2}$ from $\hat{\mathbf{X}}$,

3. *pixel-wise change detection*: deriving HR and LR change maps $\hat{\mathbf{D}}_{\text{HR}}$ and $\hat{\mathbf{D}}_{\text{LR}}$ associated with the respective pairs of observed and predicted HR and LR images, namely,

$$\Upsilon_{\text{HR}} = \left\{ \mathbf{Y}_{\text{HR}}^{t_1}, \hat{\mathbf{Y}}_{\text{HR}}^{t_1} \right\} \quad \text{and} \quad \Upsilon_{\text{LR}} = \left\{ \mathbf{Y}_{\text{LR}}^{t_2}, \hat{\mathbf{Y}}_{\text{LR}}^{t_2} \right\}.$$

Note that the *fusion* and *pixel-wise change detection* steps can be tailored by the end-user providing flexibility to better fit the target problem.

3. STATE-OF-THE-ART FUSION METHODS

This section briefly describes state-of-the-art fusion methods that are considered to perform the first step of the CD framework described in Section 2.2, specifically: Gram-Schmidt adaptive (GSA), generalized Laplacian pyramid (GLP-HS), coupled nonnegative matrix factorization (CNMF), hyperspectral superresolution (HySure)

and fast fusion based on Sylvester equation (FUSE). All methods have been extensively studied in [5] and showed the best fusion performance for several datasets. They are representative instances of different categories of fusion methods (CS, MRA, Unmixing and Bayesian) as exposed in [5]. For more information about the implementation of the aforementioned methods, the interested reader is invited to consult [5].

GSA – This CS-based method, proposed by [6] explicitly relies on the spectral response function (SRF). The computation of the synthetic intensity component, one of the basis for CS methods, is made by linear regression between the high resolution image and lower resolution bands.

GLP – The GLP method, introduced by [7] is part of the MRA methods in which spatial details in each low resolution band are obtained from the high resolution image and its low-pass versions multiplied by a gain factor. The implementation presented in [5] proposes to adopt a global gain instead of a locally one and a Gaussian filter as low-pass filtering.

CNMF – The CNMF method, proposed by [8], consists in alternately unmixing the two observed images in order to estimate the spectral signatures and the high resolution abundance maps. This method can be classified into an unmixing subdivision of subspace-based methods. The sensors characteristics SRF and PSF are incorporated into the initialization of the spectral signatures and the low resolution abundance maps, which contributes to the convergence towards a better local optimum of the cost function.

HySure – The HySure method, introduced by [9], uses total variation regularization into a subspace-based HS-MS fusion framework. This approach preserves the edges and the smoothness of homogeneous regions. The fusion task is formulated as Bayesian inference problem and solved though convex optimization.

FUSE – The FUSE method, proposed by [10], is a Bayesian approach for hyperspectral image fusion. It derives the maximum a posteriori estimator of the fused image via the exact resolution of a Sylvester equation. The prior knowledge of the relative SRF and of the PSF is required. The proposed method shows high computational performance and facilitates the addition of prior constraint information.

4. EXPERIMENTAL RESULTS

This section analyzes the performance of the CD framework when the fusion step is performed through one of the methods listed in Section 3. Real data for CD is rarely available. Thus, to quantitatively evaluate the CD framework in terms of detection performance, the simulation protocol proposed in [2] has been used to generate observed and latent images from a single reference HR hyperspectral (denoted HR-HS) image. Besides, a qualitative evaluation of the most efficient fusion methods have been conducted on two real images.

4.1. Quantitative results

Simulation protocol – The CD simulation protocol [2] requires a high spatial resolution hyperspectral (HR-HS) reference image, which is chosen as a pre-corrected $610 \times 330 \times 93$ HS image of the Pavia University, Italy, acquired by the reflective optics system

imaging spectrometer (ROSIS) sensor. Given this single HR-HS reference image, several change masks have been manually generated. For each mask, a particular type of change has been applied, for instance, by replacing the whole change mask region by different pixels, or by rotating its content. The constructed simulation dataset is composed of 15 pairs of HR-HS $\mathbf{X}^{t_i}$ and $\mathbf{X}^{t_j}$ images after and before change, with associated ground-truth change maps. Then, to generate the observed images $\mathbf{Y}^{t_1}_{\mathrm{HR}}$ and $\mathbf{Y}^{t_2}_{\mathrm{LR}}$, two different spectral degradations and one spatial degradation have been considered. The first spectral degradation corresponds to a 4-band LANDSAT MS response (Scenario 1) while the other is associated with a 43-band averaging PAN response (Scenario 2). The spatial degradation response consists in a 5×5 Gaussian blur with equal downsampling by $d = 5$ in vertical and horizontal directions. By combining and applying these spatial and spectral degradations to each image of the HR-HS pairs $\left\{ \mathbf{X}^{t_i}, \mathbf{X}^{t_j} \right\}$, HR-MS/PAN and LR-HS images $\left\{ \mathbf{Y}^{t_1}_{\mathrm{HR}}, \mathbf{Y}^{t_2}_{\mathrm{LR}} \right\}$ and their respective ground-truth change maps have been obtained. The performance of proposed fusion-based CD framework will be averaged over the whole dataset for each scenario.
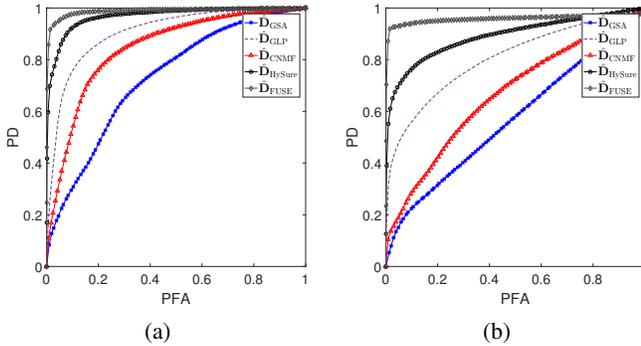

Fig. 1: Final ROC curves: (a) Scenario 1 and (b) Scenario 2.

Figures-of-merit – The detection performance assessment and the evaluation of the impact of the chosen fusion method are achieved through the receiving operator characteristics (ROC) curve, which plots the probability of the probability of detection (PD) as a function of the probability of false alarm (PFA). One of the advantages of the considered CD framework is to allow both HR and LR change maps to be derived. Based on the results reported in [2], one chooses to estimate the HR change map ($\mathbf{D}_{\mathrm{HR}}$) by conducting a component vector analysis (CVA) [11], a classical pixel-wise CD method, on the pair Υ_{HR}. Within this evaluation scenario, the CD framework is expected to perform well if the underlying fusion method produces an estimated pseudo-latent image spectrally biased to the HR image. Additionally, two quantitative measures of detection performance can be extracted from these ROC curves: the area under the curve (AUC), corresponding to the integration of the ROC curve and the distance (Dist.) between the interception of the ROC curve with the diagonal line, $\mathrm{PFA} = 1 - \mathrm{PD}$, and the no detection point ($\mathrm{PFA} = 1, \mathrm{PD} = 0$). For both criteria, the better the detection, the closer to 1 the measure.

Results – Figure 1 and Table 1 present the averaged ROC curves and associated metrics obtained with the five fusion methods for Scenario 1 (HR-MS and LR-HS images) and Scenario 2 (HR-PAN and LR-HS images). For both scenarios, FUSE and HySure methods provide the best detection performance in terms of the evaluation metrics. Note that, both techniques require a prior knowledge of SRF and PSF. Both responses are also used to predict the pseudo-

Table 1: Detection performance (AUC and normalized distance).

		$\hat{\mathbf{D}}_{\mathrm{GSA}}$	$\hat{\mathbf{D}}_{\mathrm{GLP}}$	$\hat{\mathbf{D}}_{\mathrm{CNMF}}$	$\hat{\mathbf{D}}_{\mathrm{HySure}}$	$\hat{\mathbf{D}}_{\mathrm{FUSE}}$
Sc. 1	AUC	0.728023	0.907081	0.843431	0.967933	**0.986951**
	Dist.	0.675268	0.835084	0.781578	0.912291	**0.951295**
Sc. 2	AUC	0.571118	0.80509	0.625677	0.890669	**0.957227**
	Dist.	0.542754	0.728173	0.582358	0.819382	**0.933993**

observed images in the second step of the CD framework. Besides, the ideal fusion method designed for the CD framework should produce consistent pixel values in no-change regions and aberrations in change regions. Therefore, discrepancies between the first and second steps of the CD framework may dramatically increase the number of aberrations which produce false alarms and consequently reduce the detection performance. More generally, as already mentioned before, within the adopted evaluation scenario, CD performance depends on whether the pseudo-latent image estimated by the fusion method, and thus the corresponding pseudo-observed HR and LR images, is spectrally biased. The results demonstrate the difference in the characteristics of the different fusion methods: GSA produces a fused image biased to the MS image; CNMF creates something intermediate; GLP, FUSE, and HySure produce those biased to the HS image. These characteristics play a key role in the presented CD framework although they were not significant for the conventional image fusion problem where no change is expected.
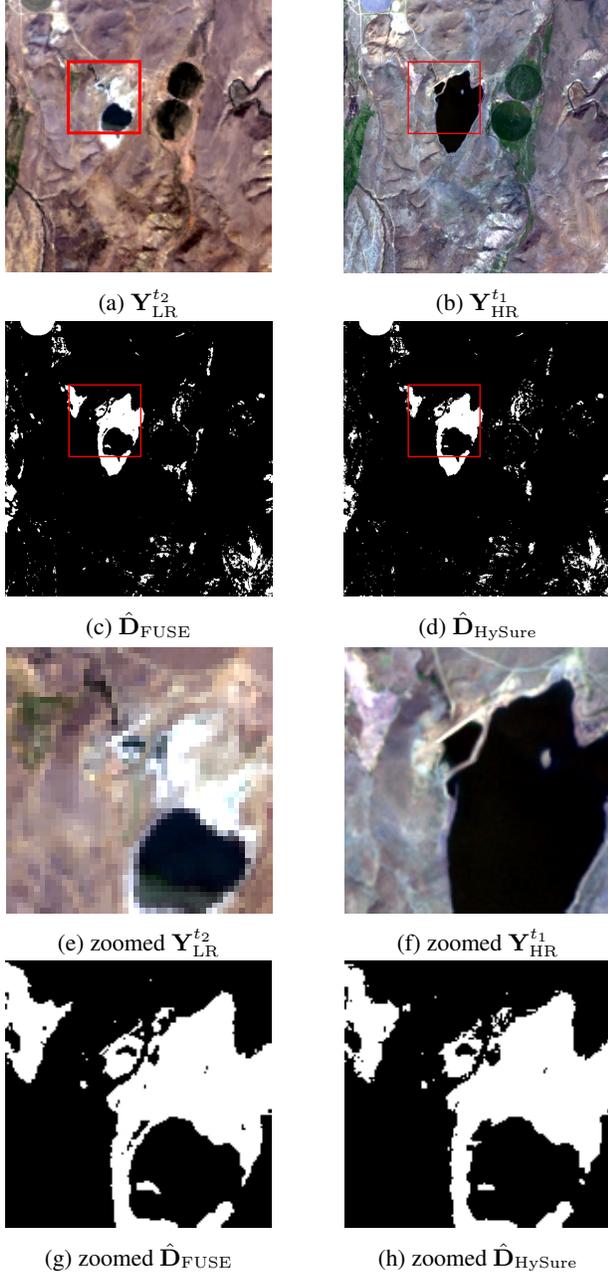
4.2. Qualitative evaluation

Finally, to compare qualitatively the detection performance of the CD framework according to a given fusion method, a pair of real LR-HS and HR-MS images acquired at different dates has been analyzed. These images $\mathbf{Y}^{t_2}_{\mathrm{LR}}$ and $\mathbf{Y}^{t_1}_{\mathrm{HR}}$ have been acquired by AVIRIS and Sentinel 2 sensors over the Lake Tahoe region (CA, USA) on September 19th 2014 and April 12th, 2016, respectively. The LR-MS image $\mathbf{Y}^{t_2}_{\mathrm{LR}}$ is of size $180 \times 175 \times 224$ characterized by a ground sampling distance (GSD) of 30m [12]. According to the spectral response of the Sentinel 2 sensor [13], the HR-MS image $\mathbf{Y}^{t_1}_{\mathrm{HR}}$ is of size $540 \times 525 \times 3$ with a GSD of 10m and has a visible RGB spectral range covering 29 bands of the LR-HS image. Fig. 2(a)–(b) shows the LR-HS and HR-MS images that have been manually geographically aligned. The resulting CD binary masks recovered by the the most efficient fusion methods identified in the previous paragraph, namely HySure and FUSE, combined with the IRMAD pixelwise CD technique [14], are depicted in Fig. 2(c)–(e).

For this pair of images, the ground truth information (i.e., in term of a binary map of actual changes) is not available. However, a visual inspection reveals that all methods succeed in recovering the most significant changes between the two images, namely, the pixels corresponding to the lake drought. Nevertheless, as pointed by the quantitative results, the FUSE method provides the highest detection rates among the tested methods, mostly by producing less false alarms. Note that, CD binary masks can be computed at HR, which helps in detecting finer details, as illustrated by the zoomed regions in Fig. 2(e)–(g).

5. CONCLUSIONS

This paper studied the appropriateness of state-of-the-art fusion methods as part of a general CD framework dedicated to multiband optical images. The comparison criterion is the final CD perfor-

tion model. The pseudo-observed images have the same resolutions as the truly observed images. The final step applies a conventional CD method to the pair of observed/pseudo-observed images in order to identify the changed pixels. Therefore, if the fusion process does not correctly produces the hybrid pixels, the detection step may not accurately detect the change regions. The CD framework was tested according to different state-of-the-art fusion methods: GSA, GLP, CNMF, HySure and FUSE. The detection performance was evaluated quantitatively and qualitatively through simulated and real images. At the end, results showed that the FUSE and HySure methods produces the highest detection performance. This result can be explained by the fact that both methods exploit the spatial and spectral response functions as prior information. Thus, when combined with the prediction step which also relies on these response functions, both methods can better succeed in producing relevant hybrid pixels and finally the accurate change map.

6. REFERENCES

[1] F. Bovolo and L. Bruzzone, "The time variable in data fusion: A change detection perspective," *IEEE Geosci. Remote Sens. Mag.*, vol. 3, no. 3, pp. 8–26, Sept. 2015.

[2] V. Ferraris, N. Dobigeon, Q. Wei, and M. Chabert, "Detecting changes between optical images of different spatial and spectral resolutions: A fusion-based approach," *IEEE Trans. Geosci. Remote Sens.*, 2017, to appear.

[3] ——, "Robust fusion of multiband images with different spatial and spectral resolutions for change detection," *IEEE Trans. Comput. Imaging*, vol. 3, no. 2, pp. 175–186, June 2017.

[4] Union of Concerned Scientists. UCS satellite database. [Online]. Available: {https://www.ucsusa.org/nuclear-weapons/space-weapons/satellite-database#.WigLykqnFPY}

[5] N. Yokoya, C. Grohnfeldt, and J. Chanussot, "Hyperspectral and multispectral data fusion: A comparative review of the recent literature," *IEEE Geosci. Remote Sens. Mag.*, vol. 5, no. 2, pp. 29–56, June 2017.

[6] B. Aiazzi, S. Baronti, and M. Selva, "Improving component substitution pansharpening through multivariate regression of ms +pan data," *IEEE Trans. Geosci. Remote Sens.*, vol. 45, no. 10, pp. 3230–3239, Oct 2007.

[7] B. Aiazzi, L. Alparone, S. Baronti, A. Garzelli, and M. Selva, "MTF-tailored multiscale fusion of high-resolution ms and pan imagery," *Photogrammetric Engineering & Remote Sensing*, vol. 72, no. 5, pp. 591–596, May 2006.

[8] N. Yokoya, T. Yairi, and A. Iwasaki, "Coupled nonnegative matrix factorization unmixing for hyperspectral and multispectral data fusion," *IEEE Trans. Geosci. Remote Sens.*, vol. 50, no. 2, pp. 528–537, Feb. 2012.

[9] M. Simões, J. Bioucas Dias, L. Almeida, and J. Chanussot, "A convex formulation for hyperspectral image superresolution via subspace-based regularization," *IEEE Trans. Geosci. Remote Sens.*, vol. 6, no. 53, pp. 3373–3388, June 2015.

[10] Q. Wei, N. Dobigeon, and J.-Y. Tourneret, "Fast fusion of multi-band images based on solving a Sylvester equation," *IEEE Trans. Image Process.*, vol. 24, no. 11, pp. 4109–4121, Nov. 2015.

[11] F. Bovolo and L. Bruzzone, "A theoretical framework for unsupervised change detection based on change vector analysis in the polar domain," *IEEE Trans. Geosci. Remote Sens.*, vol. 45, no. 1, pp. 218–236, Jan. 2007.

[12] NASA. (2017) Aviris. [Online]. Available: https://aviris.jpl.nasa.gov

[13] ESA. (2017) Sentinel 2. [Online]. Available: http://www.esa.int

[14] A. A. Nielsen, "The Regularized Iteratively Reweighted MAD Method for Change Detection in Multi- and Hyperspectral Data," *IEEE Trans. Image Process.*, vol. 16, no. 2, pp. 463–478, Feb. 2007.

(a) $\mathbf{Y}_{\mathrm{LR}}^{t_2}$ (b) $\mathbf{Y}_{\mathrm{HR}}^{t_1}$

(c) $\hat{\mathbf{D}}_{\mathrm{FUSE}}$ (d) $\hat{\mathbf{D}}_{\mathrm{HySure}}$

(e) zoomed $\mathbf{Y}_{\mathrm{LR}}^{t_2}$ (f) zoomed $\mathbf{Y}_{\mathrm{HR}}^{t_1}$

(g) zoomed $\hat{\mathbf{D}}_{\mathrm{FUSE}}$ (h) zoomed $\hat{\mathbf{D}}_{\mathrm{HySure}}$

Fig. 2: Real scenario (LR-HS and HR-HS): (a) LR-HS observed image $\mathbf{Y}_{\mathrm{LR}}^{t_2}$, (b) HR-PAN observed image $\mathbf{Y}_{\mathrm{HR}}^{t_1}$, (c) change mask $\hat{\mathbf{D}}_{\mathrm{FUSE}}$ estimated by FUSE approach, (d) change mask $\hat{\mathbf{D}}_{\mathrm{HySure}}$ estimated by HySure approach. From (e) to (g): zoomed versions of the regions delineated in red in (a)–(d).

mance. This framework relies on the presence of hybrid (resp. non-hybrid) pixels, corresponding to change (res. no-change) regions. The hybrid pixels result from the fusion of the multi-band optical images of the same scene acquired before and after a change. The framework is composed of three steps: fusion, prediction and pixel-wise change detection. The aim of the fusion step is to produce the hybrid/non-hybrid pixel map at a high resolution. The prediction step degrades the fused image according to the acquisi-